Composites: Part A 190 (2025) 108698

Contents lists available at ScienceDirect

Composites Part A

journal homepage: www.elsevier.com/locate/compositesa

Optimization of surface texturing parameters in additively manufactured continuous fiber composites using abrasive waterjet technique for composite repair applications

Arjun Chandra Shekar [a,b], Atef Sawalmeh [b], Redouane Zitoune [b,c,*], Lucas A. Hof [a,*]

[a] Department of Mechanical Engineering, École de technologie supérieure, 1100 rue Notre-Dame Ouest, Montréal, Québec, H3C1K3, Canada
[b] Institut Clément Ader (ICA), Université de Toulouse, CNRS, INSA, ISAE-SUPAERO, Mines-Albi, UPS, 3 Rue Caroline Aigle, 31400 Toulouse, France
[c] CNRS-International-NTU-THALES-Research-Alliance (CINTRA, UMI 3288), Nanyang Technological University, Singapore

HIGHLIGHTS

- Abrasive waterjet and additive manufacturing provide novel solutions for texturation.
- Waterjet pressure and traverse speed are key factors affecting surface texturation.
- Cv and Sa are more reliable surface profile metrics than Ra, Rv, and Rz.
- Texturation prediction models for Cv and Sa closely align with experimental results.
- Microscopy reveals material removal mechanisms and abrasive particle embedment.

GRAPHICAL ABSTRACT

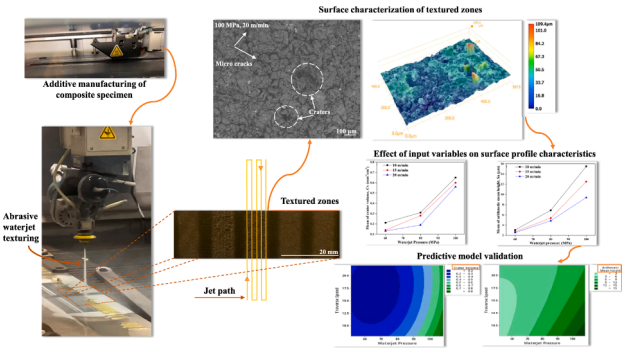

ARTICLE INFO

Keywords:
Additive manufacturing
Abrasive waterjet process
Surface quality
Composite repair

ABSTRACT

Surface texturing is critical in adhesive bonding strength, hence crucial for composite repair. This study evaluates the influence of abrasive waterjet (AWJ) machining as a texturing technique for surface preparation of additively manufactured (AM) composite parts. Effects of waterjet pressure (WP) and traverse speed (TS) on crater volume (Cv) and arithmetic mean height (Sa) were studied. Digital and electron microscopy validated surface textures, observed damage patterns, and assessed contamination due to abrasive embedment. Increasing WP from 60 to 100 MPa significantly increased Cv by 179.6 % and Sa by 410.6 %, highlighting its strong influence. In contrast, TS showed a secondary effect when increased from 10 to 20 m/min, with higher speeds producing smoother surfaces and reducing Cv and Sa by 30.78 % and 28.59 % respectively. The findings, supported by statistical analysis and multi-objective optimization, show that Cv and Sa are effective metrics for surface texture quantification in AWJ textured AM composite specimens.

* Corresponding authors.
E-mail addresses: redouane.zitoune@iut-tlse3.fr (R. Zitoune), lucas.hof@etsmtl.ca (L.A. Hof).

https://doi.org/10.1016/j.compositesa.2024.108698
Received 2 August 2024; Received in revised form 2 December 2024; Accepted 27 December 2024
Available online 28 December 2024

1. Introduction

In aerospace engineering, carbon fiber reinforced polymer (CFRP) composites emerge as distinct materials of choice, due to their remarkable properties, such as superior strength-to-weight ratio, corrosion resistance, high fatigue endurance limit, tailorable mechanical properties, thermal insulation, and design flexibility [1,2].

Despite these benefits, CFRPs are susceptible to various damage forms due to service conditions (chemical exposure, corrosion, and bird strikes), mechanical reasons (accidents, collisions, and foreign object debris) and human intervention (errors during maintenance and handling) [3,4]. These causes are detrimental not only for the structural integrity, but also to passenger safety, thus prompting stringent protocols by governing agencies such as the Federal Aviation Administration and the European Aviation Safety Agency [5,6]. These strict protocols pose operational challenges, forcing companies to choose between replacing or repairing damaged sections; each with their challenges [7]. Hence, a strategic balance between financial flexibility, sustainability, and mechanical restoration is crucial. Replacing components resolves immediate issues but generates excessive waste and contradicts circular manufacturing principles [8]. Alternatively, repair aligns with circular strategies as it emphasizes minimal waste through resource efficiency and fosters an environmentally conscious manufacturing practice [9,10].

Repairing CFRP composite structures requires the removal of material from the damaged section in order to prepare the surface for assembly of the patch [11]. Depending upon the damage severity, either machining or surface texturing can be used. Machining is preferred in the case of high volume material removal, while texturing allows finer, controlled modifications to enhance adhesion and surface interactions between the patch and the parent surface [12]. Machining and texturing are conducted by conventional milling practices in the industry [13]. However, these operations come with notable challenges [14]. Firstly, the process remains complicated due to the heterogeneous nature of CFRP composite materials [15]. Additionally, conventional milling practices for material removal often result in several types of damage, such as delamination, fiber pull-out, matrix recession, inter-laminar cracking, distortion, and thermal damage [16]. The brittle and abrasive nature of carbon fibers (CF) contribute to tool wear acceleration, thus resulting in elevated temperature and surface degradation [17]. Also, the emanation of CF dust during machining poses high risks not only to operator's health but also to the environment [12].

These concerns have prompted the industry to explore non-conventional machining techniques, such as laser and electric discharge machining as alternatives for material removal [18,19]. Regrettably, these methods also present their own operational challenges. For instance, while laser machining of CFRPs result in defects such as delamination, matrix cracking, thermal degradation and heat affected zone formation [20], electric discharge machining also has drawbacks like thermal degradation, recast layering, fiber swelling and delamination [21,22], hence limiting their usage for repair applications.

Conversely, the AWJ technique has shown tremendous potential as both an effective machining and texturing strategy in the context of composite repair [12,23]. As material removal is achieved through abrasives and water flow, issues of heat generation and emission of carbon dust are eliminated [24]. Prior research findings highlight optimization of input parameters, such as waterjet pressure (WP), traverse speed (TS), scan step (SS) and standoff distance (SoD), to achieve desired depth of material removal and surface quality, which are essential for repair applications [25]. Validation studies have further ensured agreement between the predicted and actual results through development of prediction models for critical parameters, such as material removal and surface roughness [26]. These advantages make AWJ a compelling candidate for machining and texturing operations in repair applications.

For effective composite repair, fabrication of the patch to regain the initial shape of the machined part is an important and challenging milestone to achieve [27]. In this regard, the varying designs and geometries of custom patches make it complex to adopt traditional fabrication methods, such as infusion and autoclave, among others. [28]. These methods may lead to higher processing times and material wastage to achieve the desired form and shape. On the contrary, additive manufacturing (AM) offers distinct advantages particularly during patch fabrication, due to its nature of material deposition [29]. Through precise modeling of the patch design in 3D, the actual replicate of the cavity, i.e. the repair patch, may be seamlessly reproduced externally by employing a reliable AM technology like material extrusion (MEX) [30,31]. This fabrication method has the potential to realize intricate designs with precision while minimizing material wastage. In this context, MEX technology may be extended to the development of repair patches. With recent advancements in continuous fiber filament technology, emphasis may be given to the exploration of thermoplastic based AM approaches for composite materials to facilitate the research and development of customizable patches for repair [32]. This combination of using continuous CF technology with thermoplastics within AM technology potentially revolutionizes the way repair is viewed in the realm of aerospace maintenance repair and overhaul.

It is visualized that the integration of AWJ and MEX offer superior advantages for composite repair research. It is believed that this synergy has the potential to deliver sustainable and comprehensive repair solutions, promoting circularity in manufacturing through service life prolongation of composite structures. Therefore, the authors consider it important to explore this original and innovative solution as there is an absence of similar work in the available literature. The spirit of this research is to support informed decision-making and develop optimized strategies for addressing advanced mechanical engineering challenges through circular economic practices.

In the present study, the effect of surface texturing on MEX fabricated composite materials using the AWJ process is explored. The objective is to analyze the influence of AWJ input variables on the surface texture of the material. Through a design of experiments approach, multiple experiments are conducted to assess surface texture variations under different texturing conditions. Scanning electron microscopy (SEM) and digital microscopy are employed to examine the underlying material removal mechanisms and validate experimental findings. Additionally, contamination analysis is conducted to quantify the embedment of abrasive particles within the textured surface. Analysis of Variance (ANOVA) is utilized to determine the significance of input parameters on surface profile parameters. Furthermore, the response surface methodology is employed for multi-objective optimization to assess the interaction effects between input and output variables. It is anticipated that this research will provide valuable insights into surface texturing for composite repair, particularly in scenarios involving AM and AWJ machining.

2. Materials and experimentation

2.1. Composite materials

The study employs a Markforged Mark-Two 3D printer, which combines MEX and continuous filament fabrication methodology.

Table 1
Specifications and printer settings configured in Eiger software.

Printer Settings	Specifications	Printer Settings	Specifications
Heat bed temperature	Not heated	Pattern of fill	Solid
Fiber nozzle temperature	272 °C	Print infill density	100 %
Matrix nozzle temperature	253 °C	Layer thickness	0.125 mm
Total fiber layers	10	Floor layers	2
Total matrix layers	8	Roof layers	2
Fiber fill type	Isotropic	Wall layers	1
Concentric fiber rings	1	Fiber angle	0°

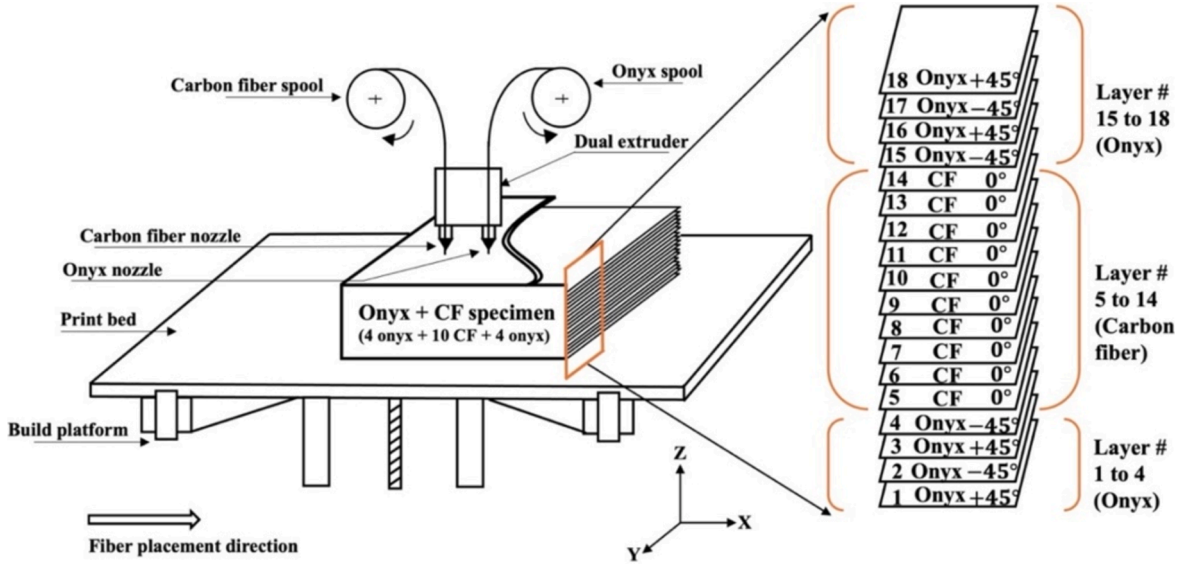

Fig. 1. Illustration of the composite 3D printer with the stacking sequence strategy.

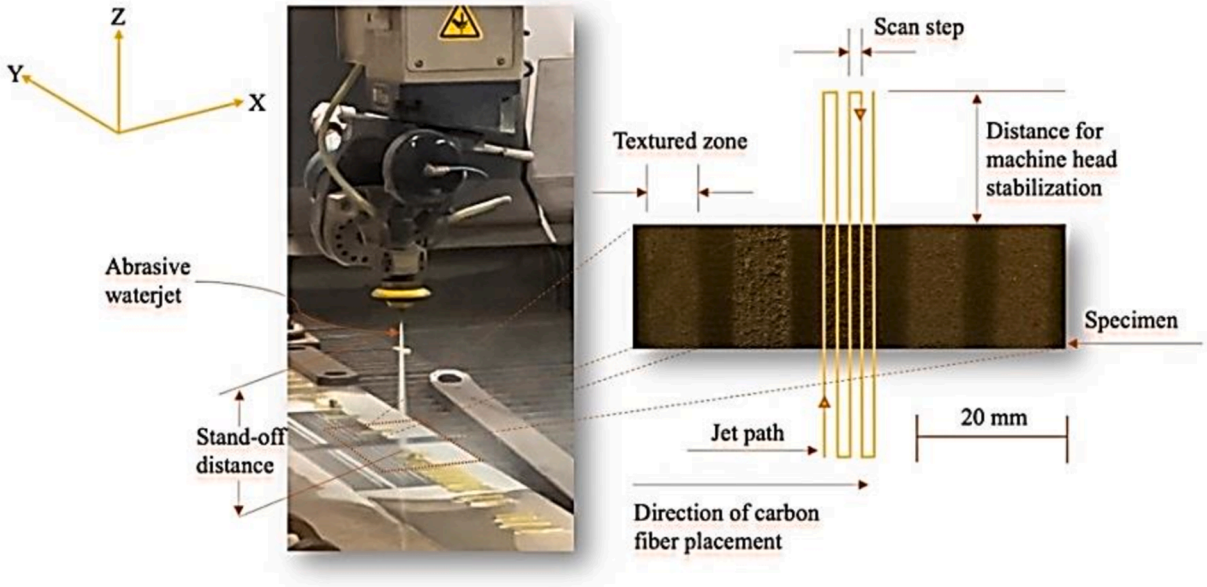

Fig. 2. Abrasive water jet texturing process and key nomenclature used in this work.

Specimens were printed using continuous CF as reinforcement and onyx thermoplastic as matrix material, both sourced from Markforged corporation. The printer settings were configured using the company's proprietary software 'Eiger' and the specifications are listed in Table 1.

Three rectangular specimens, each measuring 300 mm in length, 20 mm in width and 2.25 mm in thickness, were printed. The selected thickness of 2.25 mm is representative of the fuselage panel thickness of aircrafts, such as the Airbus A350. The onyx – CF composite material attained a fiber volume fraction of approximately 56 %, calculated using an approach aligned with prior research work [33].

The printing process is as illustrated in Fig. 1. The composite specimens are fabricated with a specific stacking sequence where the first and last four layers printed with onyx are set at ±45°, aligning with the printer's default settings. The central ten layers impregnated within onyx are printed with CF and are oriented at 0° to optimize the composite's mechanical properties [34].

2.2. Surface texturing using AWJ

Surface texturing was performed using a Mach 4c AWJ machine from Flow International corporation. The machine is equipped with a Hyplex pump and Paser 4 nozzle. The focusing tube diameter and length are 1.016 and 76 mm respectively. The nozzle diameter is 0.3302 mm and the abrasive flow rate is 0.18 Kg/min. 120 mesh size garnet sand abrasive particles were sourced from Wuxi Ding Long Minerals Ltd., China. During texturing, a raster scan pattern strategy was employed along the y-direction as shown in Fig. 2. Additionally, a deliberate jet traverse extension of 100 mm was included on either side of the specimen to mitigate excessive material erosion. This extension served to counteract the changes in the machine head induced by the reversal in direction between passes of the jet traverse. This length was determined through iterative testing, where different extension lengths were studied to minimize erosion, and 100 mm was found to be optimal in stabilizing the machine head.

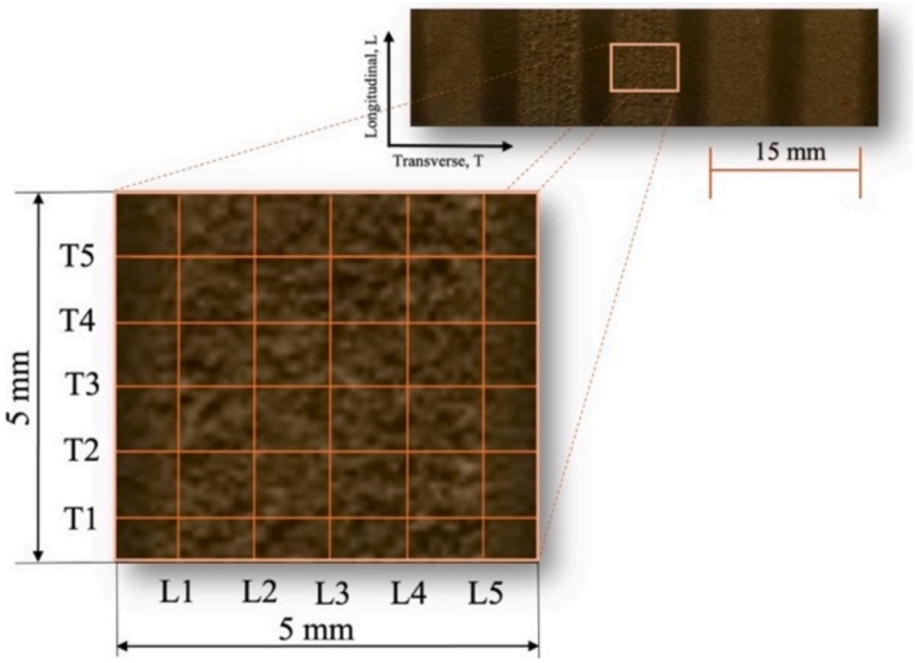

Fig. 3. Textured surface profile zone for measurements within 5 × 5 mm^2 at the center of the total 5 × 20 mm^2 (inset). L1 to L5 indicate the parallel sides, while T1 to T5 are perpendicular sides.

From previous studies, it is established that WP, TS, SS and SOD significantly influence the surface texturing quality in AWJ machining [12,23]. The range of these variable input parameters was selected based on similar published research [24]. Water jet pressure was varied in increments of 10 MPa from 50 MPa to 120 MPa, traverse speed in steps of 5 m/min from 5 m/min to 20 m/min, scan steps from 0.5 mm to 1.5 mm, and the stand-off-distance from 50 mm to 150 mm. Multiple iterations were conducted in these ranges to correlate the effect of each parameter with the surface texturing which is discussed in detail in the subsequent sections.

2.3. Characterization

2.3.1. Surface topology acquisition

Surface topography was acquired using an Infinite Focus SL optical surface profilometer from Alicona corporation.

The objective lens was fixed at 10× with 0.1 μm vertical and 2.0 μm lateral resolution. The total scanned surface area was 5 × 20 mm^2 and the measured surface area was the central 5 × 5 mm^2 as shown in Fig. 3.

2.3.2. Surface quality

Quantification of surface quality was performed using Alicona software. Cv was determined by measuring the void regions located underneath the mean least square plane. To mitigate the edge effects arising from the entry and exit of the jet upon the surface under consideration, the measurement area was fixed to the central zone as shown in Fig. 3. Subsequently, the volumes of craters were normalized by the total scanned surface to facilitate comparison across specimens and conditions. Additionally, the arithmetic mean height (Sa) was acquired within the same measurement zones. Introducing Cv and Sa as complementary metrics provides a holistic approach to characterizing surface textures in AWJ treated composites. Cv and Sa together capture both the cratered profile and the average surface height, thus providing a comprehensive understanding of the surface characteristics.

2.3.3. Defect characterization and 3D profile quantification

The textured samples were examined under dry conditions using a Keyence digital microscope (Model: Keyence VHX-7000, Japan). The 3D profile height of the textured surface was reconstructed from multiple focused images at different heights, creating a stitched 3D color image with a scale bar. A Hitachi TM 3000 SEM equipped with back scattered electron (BSE) mode was utilized to detect and analyze machining-induced defects on the textured surfaces. By processing these BSE images using ImageJ software and examining the energy-dispersive X-ray spectroscopy (EDX) report, the area that was contaminated by abrasive particles was quantified.

3. Results and discussion

3.1. Abrasive water jet texturing (AWJT)

To establish the influence of AWJ input variables on surface texturing, various surface qualities were produced by varying WP, TS, SS and SoD. Iterative experimentation showed that SoD at 125 mm resulted in sparse material removal, while 75 mm resulted in uneven surface texturing (Fig. 4a–c). It was observed that SoD values at 100 mm demonstrated uniform surface texture. Further, an SS of 0.5 mm caused excessive material removal, and 1.5 mm led to incomplete surface texturing (Fig. 4d–f). An SS at 1 mm provided optimum surface texture. Prior research indicates that SS and SoD minimally affect material removal compared to WP and TS [23,25]. Therefore, a constant SS of 1 mm and SoD of 100 mm were maintained throughout the study for consistency (Fig. 4g) [25].

It is well established that WP and TS are the dominating factors influencing material removal behaviour [23,35], a principle that extends to surface texturing as well. In incremental steps of 10 MPa WP and 5 m/min TS, preliminary studies were undertaken to study the influence of WP and TS on surface texturing. Observations during these trials showed negligible texturing below 50 MPa and significant damage to sample integrity when WP exceeded 100 MPa, motivating the selection of WP values between 50 and 120 MPa. Similarly, TS levels below 10 m/min caused excessive texturing, while values above 20 m/min resulted in insufficient contact time for effective texturing. Based on these observations, WP levels of 60, 80 and 100 MPa and TS of 10, 15 and 20 m/min were selected as variable parameters through iterative experimentation and prior understanding of material removal behavior

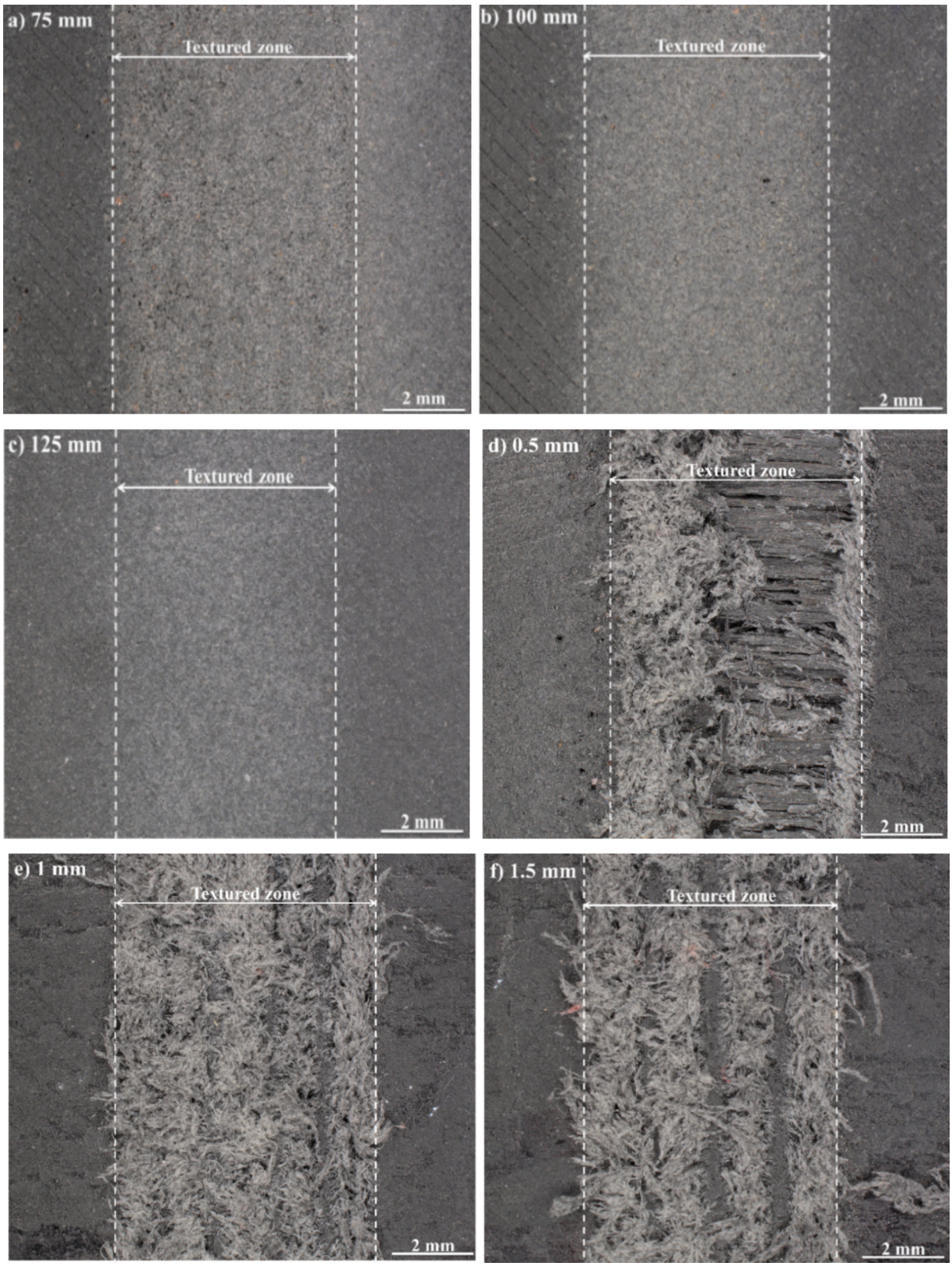

Fig. 4. Micrographs of MEX samples subject to AWJ texturing at constant WP = 100 MPa, TS = 10 m/min with (a–c) varying SoD, (d–f) varying SS and (g) at optimum conditions.

[36,37]. The corresponding AWJ velocities, calculated at each pressure level based on the work of Hashish [38], were 224.47 m/s, 259.20 m/s and 289.79 m/s for 60, 80, and 100 MPa, respectively.

3.2. Effect of input variables on the surface texturing based on design of experiments

In this section, details on the impact of AWJ input variables on the

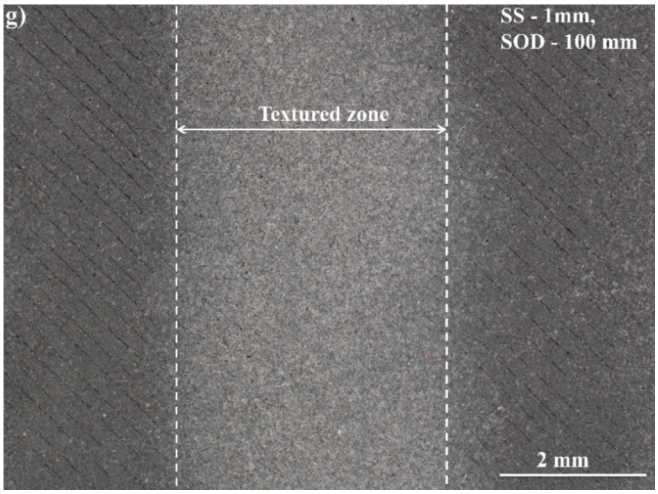

Fig. 4. (*continued*).

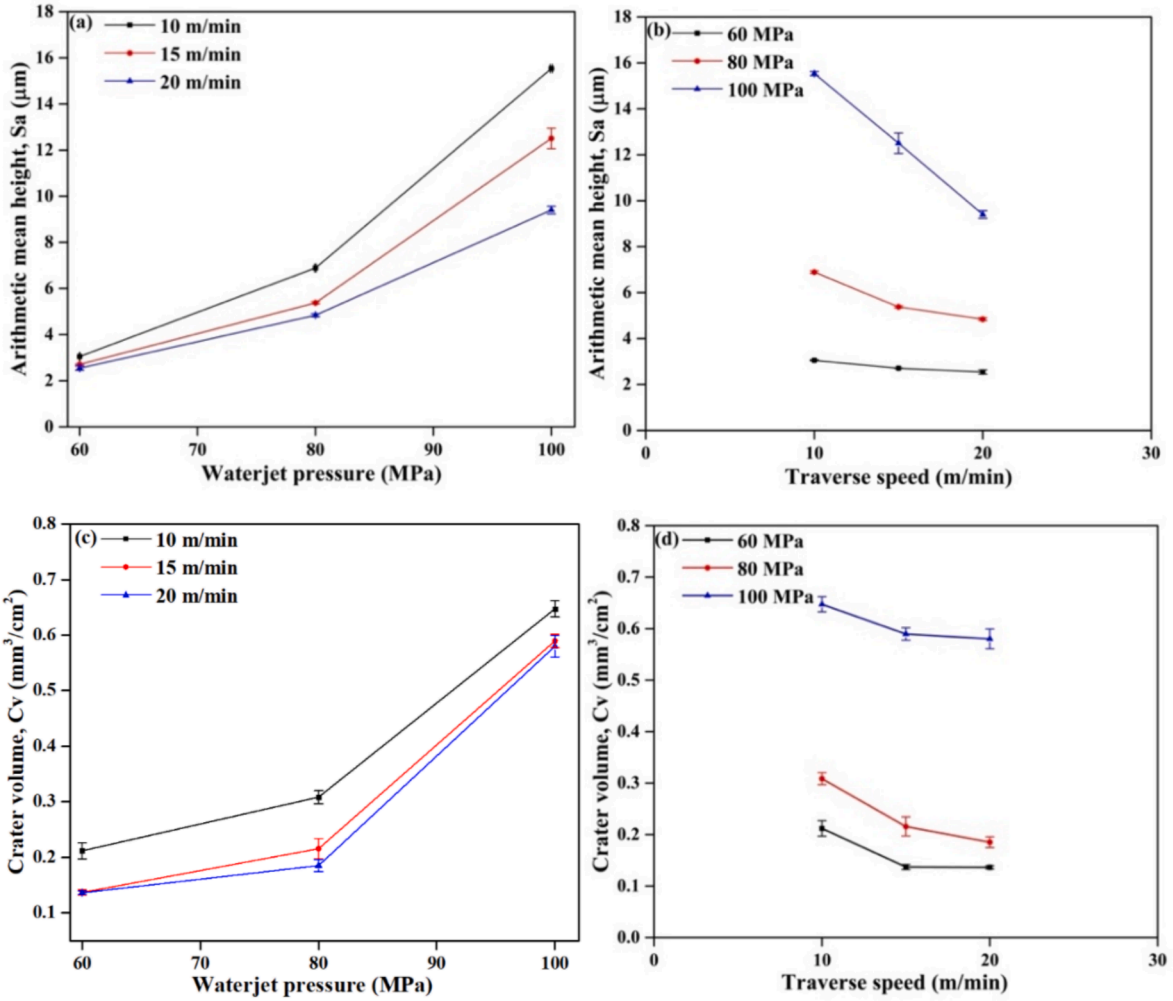

Fig. 5. Variation of arithmetic mean height (Sa) with (a) WP (b) TS; Variation of crater volume (Cv) with (c) WP (d) TS.

surface texturing outcomes are discussed. As established earlier, WP and TS are selected as the two input variables. By adopting a design of experiments approach, 27 trials were designed ensuring three repetitions to evaluate the effects of varying WP (60, 80 and 100 MPa) and TS (10, 15 and 20 m/min). To assess the textured surface characteristics, Cv and Sa are chosen as the output parameters. These parameters offer superior representation compared to other measurement metrics, such as arithmetic average roughness (Ra), maximum profile valley depth (Rv) and ten points mean roughness (Rz), in quantifying texturing effects on additively manufactured materials subjected to AWJ [24]. The rationale

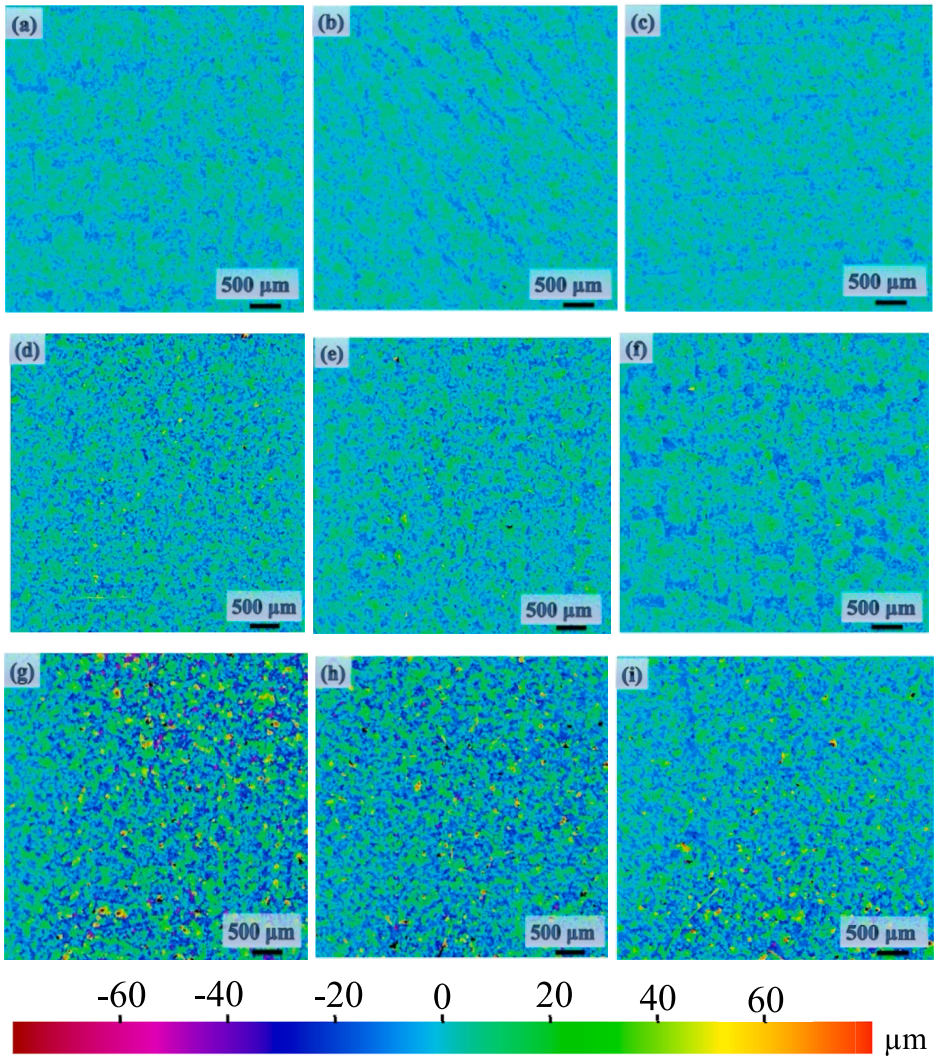

Fig. 6. Surface profile cartographies with constant SoD (100 mm) and SS (1 mm), varying WP and TS: (a) 60 MPa, 10 m/min; (b) 60 MPa, 15 m/min; (c) 60 MPa, 20 m/min; (d) 80 MPa, 10 m/min; (e) 80 MPa, 15 m/min; (f) 80 MPa, 20 m/min; (g) 100 MPa, 10 m/min; (h) 100 MPa, 15 m/min; (i) 100 MPa, 20 m/min. Color bar shows height profile in micrometers.

for selecting Cv and Sa over other classical surface profile parameters is discussed in section 3.4.

The effect of varying WP on Sa is as shown in Fig. 5a. At 60 MPa WP and 10 m/min TS, Sa value of 3.03 µm may be observed, while at 100 MPa WP and 10 m/min TS, it increases to 15.49 µm. This high change of 410.6 % increase confirms the direct proportionality effect of WP on Sa. When seen from the TS viewpoint (Fig. 5b), at 10 m/min TS and 100 MPa WP, the value of Sa is 15.49 µm whereas at 20 m/min TS and 100 MPa WP, it reduces to 9.39 µm. A percentage drop of −39.3 % is observed with increase in TS, indicating an inverse relationship between TS and Sa. The difference in magnitude of percentage change signifies that WP has superior influence in surface texturing in comparison to TS. The decreasing trend in Sa with increasing TS, from 10 m/min to 20 m/min, highlights how increased TS leads to reduction in average height of the surface profile, indicative of smoother surface profiles [25]. The observed decrease in Sa with increasing TS can be attributed to reduced contact time of the AWJ on each point on the composite surface [39].

Fig. 5c illustrates the relationship between Cv and WP across varying TS of 10 m/min, 15 m/min, and 20 m/min. The trend indicates that an increase in WP lead to higher Cv values, emphasizing its significant effect on Cv across all traverse speed conditions. An increase in pressure leads to higher kinetic energy of water and abrasive particles, thereby increasing impact energy. This enhanced energy facilitates deeper penetration of abrasive particles, resulting in greater material removal and pronounced crater formation [25]. However, the difference in Cv between TS values of 15 m/min and 20 m/min is minimal, indicating a plateau in material removal volume at higher TS thresholds, due to reduced interaction time between the AWJ and the composite surface as seen in Fig. 5d.

For a given TS condition, it may be observed that an increase in WP leads to increase in Cv. At 10 m/min TS, the Cv value increased from 0.22 mm^3/cm^2 at 60 MPa to 0.63 mm^3/cm^2 at 100 MPa marking a 179.6 % increase. While TS also impacts the Cv, its effect appears less pronounced compared to WP. Higher TS ranges contribute to the formation of shallower craters due to reduced interaction time between the AWJ and the material surface as illustrated in Fig. 6. For instance, at a WP of 100 MPa, the Cv decreases from 0.63 mm^3/cm^2 at 10 m/min TS to 0.57 mm^3/cm^2 at 20 m/min TS. This trend indicates a smaller percentage variation of −8.3 % reiterating the inverse relationship between TS and Cv, i.e., higher speeds resulting in lower Cv values. In summary, the analysis of WP and TS in relation to Cv and Sa highlights WP as the primary influential factor in determining output variables. The substantial percentage differences across varied WP levels in contrast to that of TS, emphasize WP's primary significance in surface characterization of MEX composite texturing. While TS also affects the output variables, its influences is secondary to that of WP.

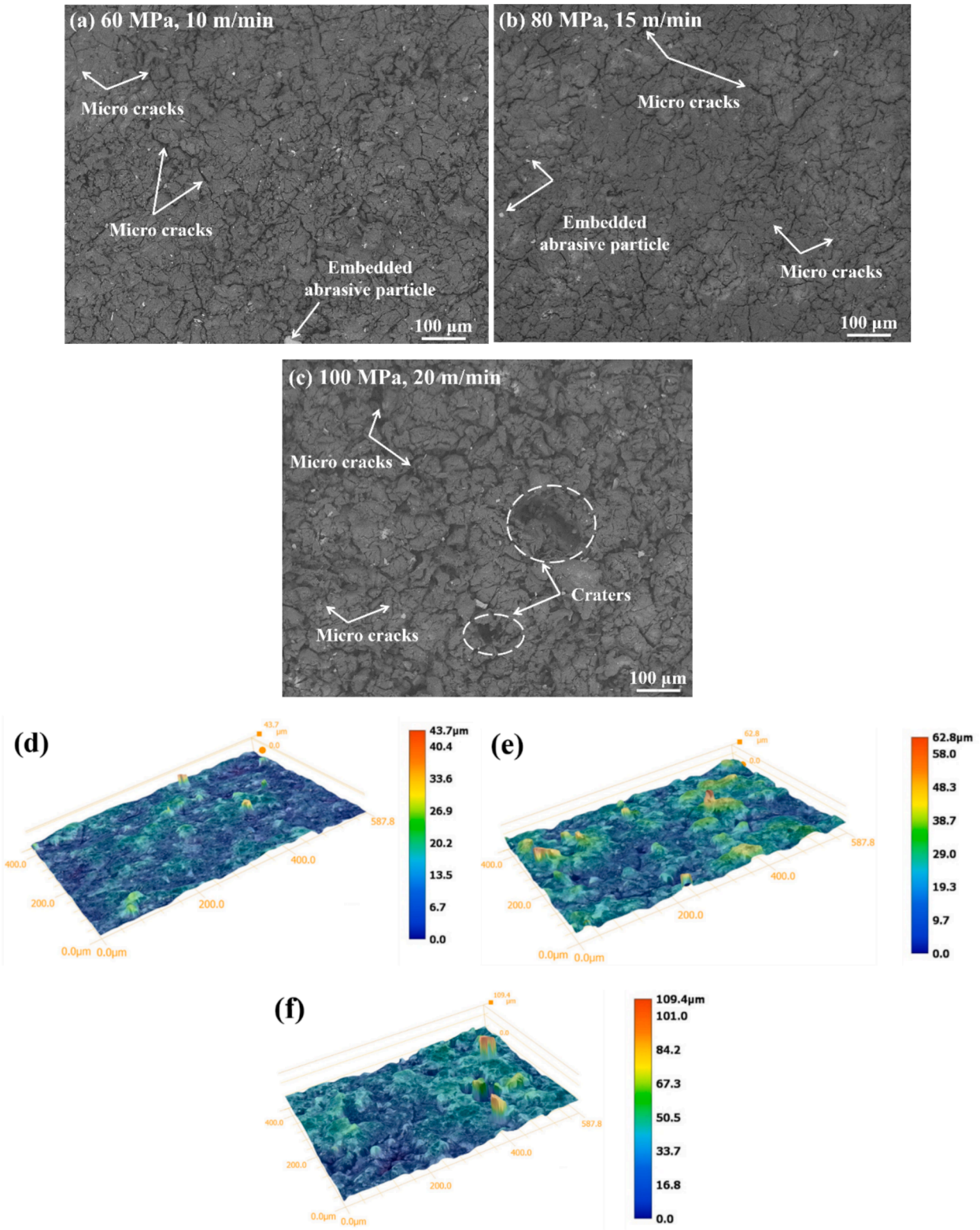

Fig. 7. Micrographs (a–c) and corresponding 3D height profiles (d–f) of textured samples subjected to different WP and TS: (a and d) 60 MPa, 10 m/min; (b and e) 80 MPa, 15 m/min; (c and f) 100 MPa, 20 m/min.

Surface texture cartographies obtained post texturing is presented in Fig. 6(a–i). Observed material removal trends highlight the individual and combined influence of WP and TS on surface texturing. As shown in Fig. 6(a–c), the intensity in material removal decreases with increasing TS at a constant WP of 60 MPa. This trend is consistent at higher pressures as well. Higher pressures intensify surface texturing, evident in the increased intensity at 80 MPa (Fig. 6d–f) and 100 MPa (Fig. 6g–i) compared to 60 MPa. The relationship between WP and TS crucially dictates the composite surface texture. The impact energy from WP and surface contact time from TS drive this relationship. Lower WP with higher TS results in smoother surfaces (Fig. 6c), while higher WP with lower TS leads to maximum material removal and surface irregularities

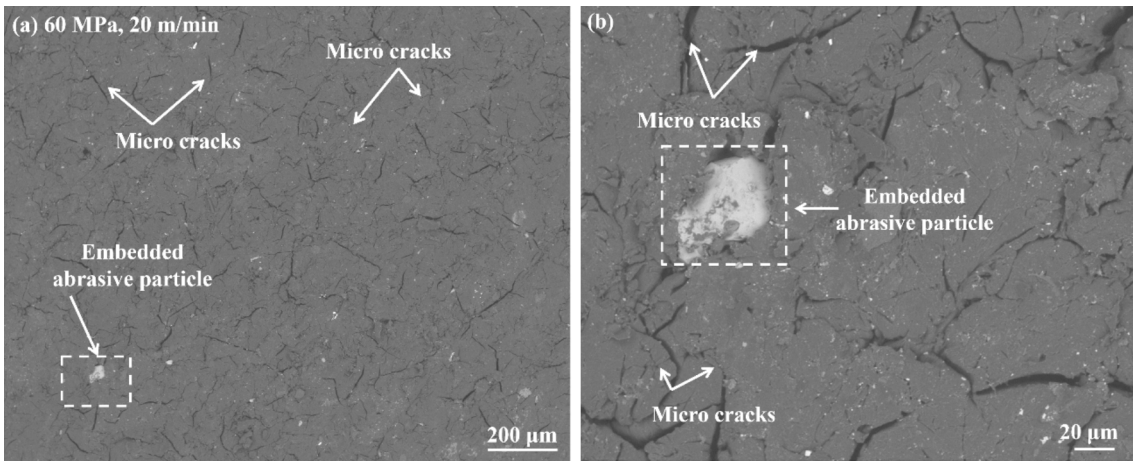

Fig. 8. (a, b) Formation of cracks and abrasive embedment at WP = 60 MPa and TS = 20 m/min at different magnifications.

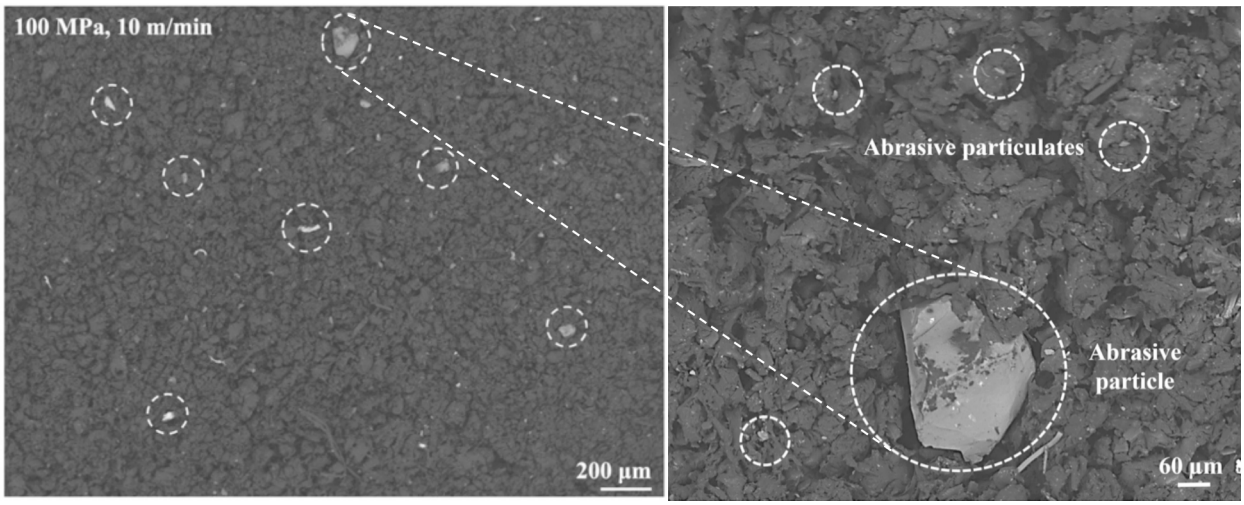

Fig. 9. SEM micrographs of textured samples at WP = 100 MPa and TS = 10 m/min. The main image highlights an overview of the abrasive particulates, with an inset at higher magnification illustrating abrasive particulate embedment.

(Fig. 6g).

3.2.1. Mechanism of material removal

Using SEM and digital microscopy, the interactions between WP and TS on surface texturing were analysed. At a lower WP (60 MPa), the predominant mechanism of material removal involves micro cracking as described in Figs. 7(a) and 8. The corresponding 3D surface profiles (Fig. 7d) exhibit uniformity, although with some elevated regions, likely due to embedded abrasive particles. The color intensity maps (Fig. 6a and c) show deeper profiles at 10 m/min TS in comparison to 20 m/min TS, indicating higher material removal, although the overall material removal at this WP level is smaller due to the lower pressure.

Similar trends may be observed at 80 MPa WP, with more pronounced surface cracking and increased surface irregularities (Fig. 7b and e). The increased presence of craters and ridges in the 3D surface profile corroborates enhanced surface texturing characteristics attributed to higher WP. Furthermore, the effects observed at 100 MPa follow the same trend, but with greater crater volumes and thicker microcracks as prominently visible from Fig. 7(c and f). The 3D height profiles display the transition in surface irregularities from low to high, indicative of deeper penetration and embedment of abrasive particles, due the higher WP. The analysis of SEM micrographs and 3D surface profiles highlights the intricate relationship between process variables and material removal mechanisms, providing valuable insights for surface texture optimization of MEX fabricated continuous fiber composites textured by AWJ.

3.3. Contamination analysis

As the hardness of garnet abrasive particles is greater than the onyx matrix of the AM composite, surface contamination by grain embedment is inevitable. Despite the flushing out of loose abrasive particles during secondary jet passes, a small portion of deeply lodged abrasive particles, due to matrix porosity and the soft nature of the AM fabricated matrix, persist within the composite. Fig. 9 highlights a global view of the scattered abrasive particulates in an approximately 4 × 4 mm^2 focus zone along with a magnified section indicating the presence of abrasive particulates embedded within the matrix.

SEM analysis in BSE mode was used to investigate this phenomenon. Heavier abrasive particles (rich in Si) appear brighter due to their higher atomic number compared to the onyx matrix (Fig. 9). These embedded particles, significantly smaller than the initial 125 µm size and exhibiting sharp edges, confirm fragmentation within the mixing chamber or upon impact. Similar observations are reported in earlier work on 3D woven composites and fiber metal laminates [16,32]. This research also explores the relationship between the nozzle diameter and scan step's influence on contamination. It was shown from earlier work that a scan step of 1 mm for a nozzle diameter of 1.016 mm facilitated least

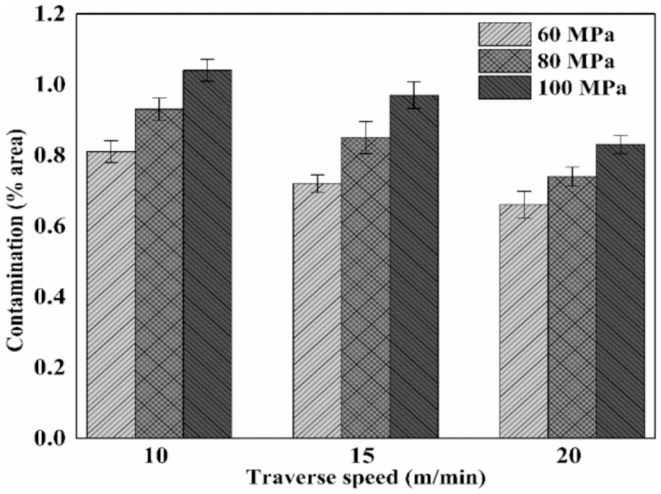

Fig. 10. Percentage of contamination at varying waterjet pressure (WP) and traverse speeds (TS).

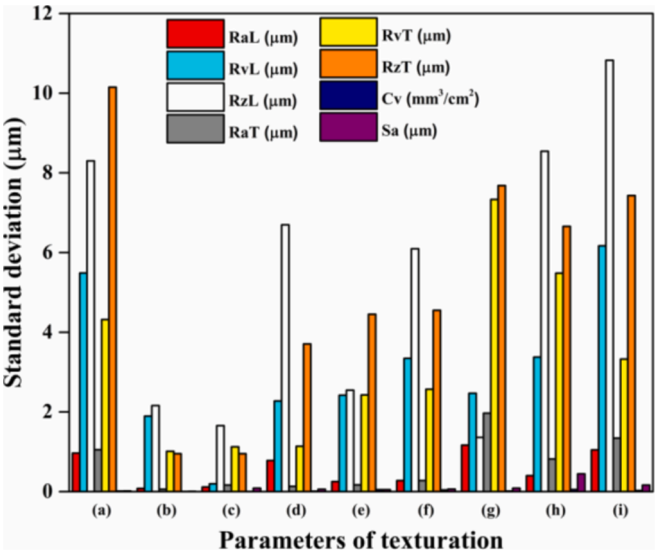

Fig. 11. Standard deviation of RaL, RvL, RzL, RaT, RvT, RzT, Cv and Sa at constant SS – 1 mm and SoD – 100 mm with variable WP and TS: (a) 60 MPa, 10 m/min; (b) 60 MPa, 15 m/min; (c) 60 MPa, 20 m/min; (d) 80 MPa, 10 m/min; (e) 80 MPa, 15 m/min; (f) 80 MPa, 20 m/min; (g) 100 MPa, 10 m/min; (h) 100 MPa, 15 m/min; (i) 100 MPa, 20 m/min.

contamination [40]. The same conditions were applied in the current research study as well. The contamination analysis shows that the intensity of the abrasive particle deposition on the composite specimen is significantly influenced by both WP and TS. As it can be observed from Fig. 10, higher WP consistently leads to increased deposition, due to the greater energy transfer from the jet to the abrasive particles, resulting in intense bombardment and thus, embedment of abrasive particles onto the surface. TS has a secondary effect on contamination: at lower speeds (10 m/min), the contamination is higher due to the prolonged interaction time, allowing more particle embedment into the surface. At a 15 m/min TS; the contamination is relatively lower, potentially due to an optimal balance where the primary jet allows effective particle embedment, while the secondary jet aids in flushing out the loose particles. At higher speeds (20 m/min TS), contamination is relatively minimized as the reduced contact time between the jet and the surface prevents prolonged particle interaction and allows the faster traverse movement to carry abrasive particles away rather than lodging them in the surface. Additionally, supporting factors including enhanced flushing action, and changing dynamics of particle impact at higher TS, result in more superficial interactions. Factors contributing to contamination also include the composite's soft and porous matrix, its non-homogeneous nature, porosity introduced by the MEX process, and the impact energy associated with the jet. Although contamination is an inevitable drawback of the AWJ methodology, optimizing the WP and TS parameters can significantly mitigate its impact.

3.4. Developing an optimal surface characterization approach: Rationale for texturing in repair applications

The surface characterization conducted in this study focuses on the assessment of textured zones using surface profiling parameters, Sa and Cv. It has to be noted that since Ra, Rv, and Rz are two-dimensional parameters [41], their capture is also included in this comparative analysis. Indeed, inclusion of these parameters provide a broader comparative analysis, particularly relevant to composite materials, as they are commonly used metrics in the field [24]. These surface parameters are captured in both longitudinal and traverse direction, represented by the letters 'L' and 'T' respectively, as presented in Table S.1 in the Supplementary Information. While prior research has predominantly focused on RaL, RaT, Sa, and Cv for 3D woven composites [24], the present study also extends the analysis to include Rz and Rv as well, aiming to capture finer surface details and evaluate their efficacy in surface characterization. The findings indicate a crucial distinction among surface roughness parameters, particularly concerning their standard deviation values across different texturing conditions as described in the Fig. 11. Notably, Cv and Sa emerge as the most suitable parameters for characterizing the material, as evidenced by consistently low standard deviation values across all texturing conditions. In contrast, parameters such as Ra, Rz, and Rv (along both longitudinal and traverse directions) exhibit considerable variability, rendering them less effective for capturing the intricate surface characteristics of the material.

On the contrary, the consistency offered by Cv and Sa enhances the confidence in experimental findings and facilitates meaningful comparisons across different surface textures. The disparities in standard deviation values observed across these classical surface roughness parameters can be attributed to various technical intricacies inherent to both the AWJ texturing process and the characteristics of AM with MEX. The localized variations in abrasive flow during AWJ texturing pose challenges in precisely quantifying the exact flow targeted to specific regions, resulting in inconsistent surface textures. Parameters such as Ra, Rz, and Rv are driven by these changes, hence susceptible to these variations, leading to scattered standard deviation readings. Conversely, Cv and Sa, which consider comprehensive surface features and overall texture uniformity despite localized fluctuations in abrasive flow, demonstrate lower standard deviation values due to their ability to capture holistic surface characteristics [23]. Also, the inherent surface unevenness within the MEX prints, characterized by density and porosity differences, enhances the variability in standard deviation values across different texturing conditions. This combined effect, arising from both the texturing process and the inherent material properties, poses challenges for classical parameters for accurate surface quality characterization, making Cv and Sa reliable strategies for surface texture quantification.

3.5. ANOVA analysis

An ANOVA analysis was performed to evaluate the effects of input parameters and validate the statistical significance of the experimental results. The design matrix and resultant output responses for Cv and Sa across the textured conditions, listed in Table 2 based on Design of Experiments (DOE), are discussed in this section. The analysis, conducted using Minitab software, aimed to validate the adequacy of the obtained

Table 2
Experimental matrix and results of the performed ANOVA analysis.

Run Order	Waterjet Pressure (MPa)	Traverse Speed (m/min)	Cv (mm^3/cm^2)	Sa (μm)
1	60	10	0.226	3.034
2	60	15	0.143	2.707
3	60	20	0.135	2.502
4	80	10	0.301	6.866
5	80	15	0.252	5.423
6	80	20	0.186	4.795
7	100	10	0.632	15.498
8	100	15	0.608	12.810
9	100	20	0.579	9.396
10	60	10	0.213	3.065
11	60	15	0.133	2.716
12	60	20	0.120	2.650
13	80	10	0.302	6.845
14	80	15	0.287	5.368
15	80	20	0.144	4.912
16	100	10	0.650	15.635
17	100	15	0.610	11.992
18	100	20	0.546	9.568
19	60	10	0.196	3.060
20	60	15	0.145	2.707
21	60	20	0.135	2.487
22	80	10	0.328	6.957
23	80	15	0.298	5.327
24	80	20	0.225	4.822
25	100	10	0.661	15.469
26	100	15	0.575	12.707
27	100	20	0.552	9.237

model for each response to ensure the statistical accuracy of the experimental results. A multilevel factorial design was employed, involving two factors: WP (at 60, 80, and 100 MPa) and TS (at 10, 15, and 20 m/min), each comprising three levels. With three replicates for each factor combination totaling 27 runs, the experimental design allowed for comprehensive exploration of the effects of these factors on surface characteristics.

The contour and surface plots, presented in Fig. 12, show the combined effects of WP and TS on Cv and Sa. The ANOVA results for Cv and Sa provide more detailed and in-depth insights into the studied surface texturing processes. Both models exhibit highly significant 'F' values of 2281.48 for Sa and 309.00 for Cv ($P < 0.05$), highlighting their robust statistical significance and validating their efficacy at a 95 % confidence level. Across both analyses, each individual factor, i.e., linear effects of WP, TS, and their interactions, significantly contributes to the variability observed in the respective surface characteristics. Specifically, the linear effects of WP demonstrate substantial influence, with 'F' values of 7987.69 for Sa and 1175.91 for Cv, along with TS effects of 678.78 and 53.43, respectively. Additionally, the low error terms of 0.503 for Sa and 0.000410 for Cv suggest minimal unexplained variability in the models, increasing confidence in their predictive accuracy. The obtained ANOVA results confirm the significance of WP and TS on Sa and Cv, given the resulting low p-values.

3.6. Multi response optimization of Cv and Sa

In this study, a Central Composite Design was employed to investigate the effects of WP and TS on the response variables, focusing on achieving maximum, minimum and targeted values of Cv and Sa. This was followed by Response Surface Methodology (RSM) analysis to

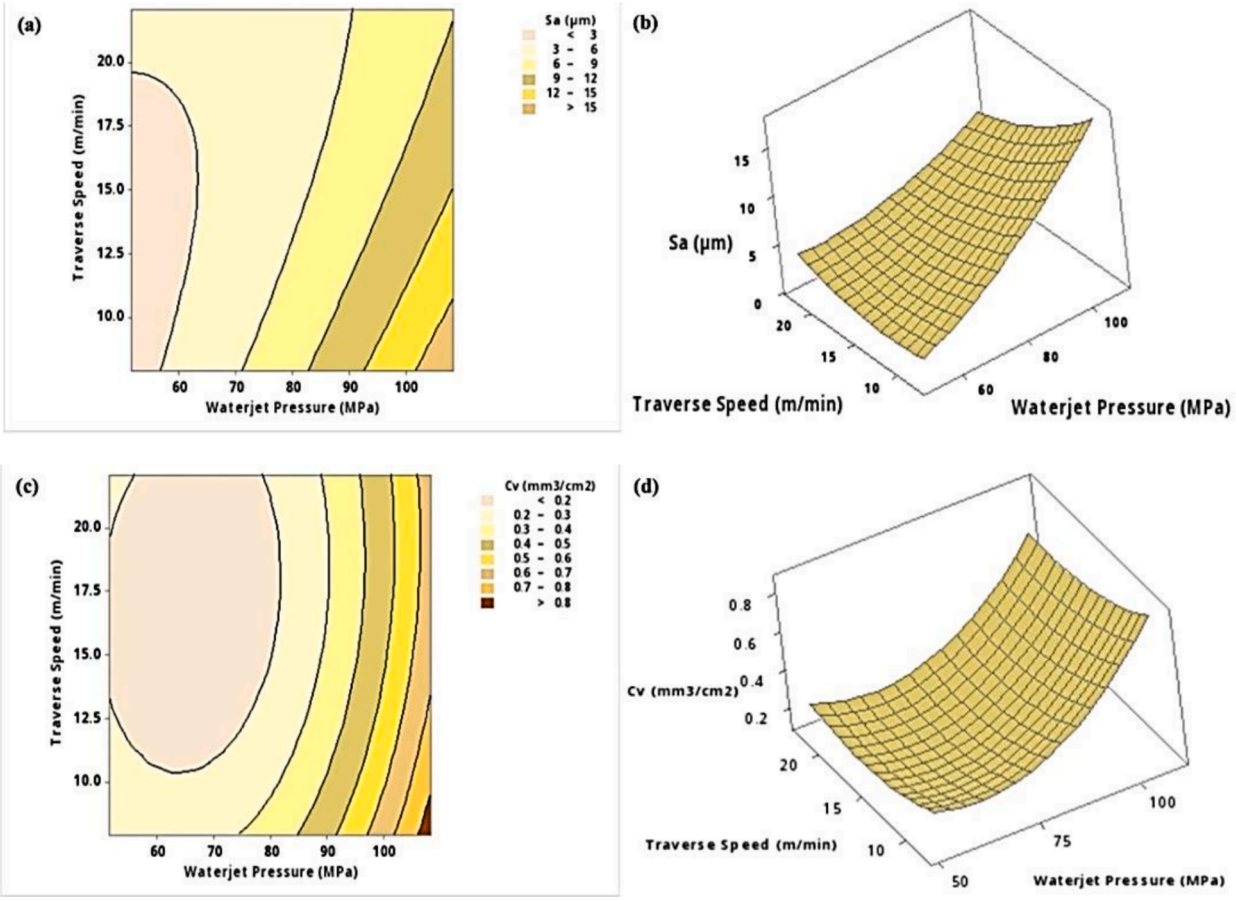

Fig. 12. Contour and surface plots of Sa and Cv for varying WP and TS.

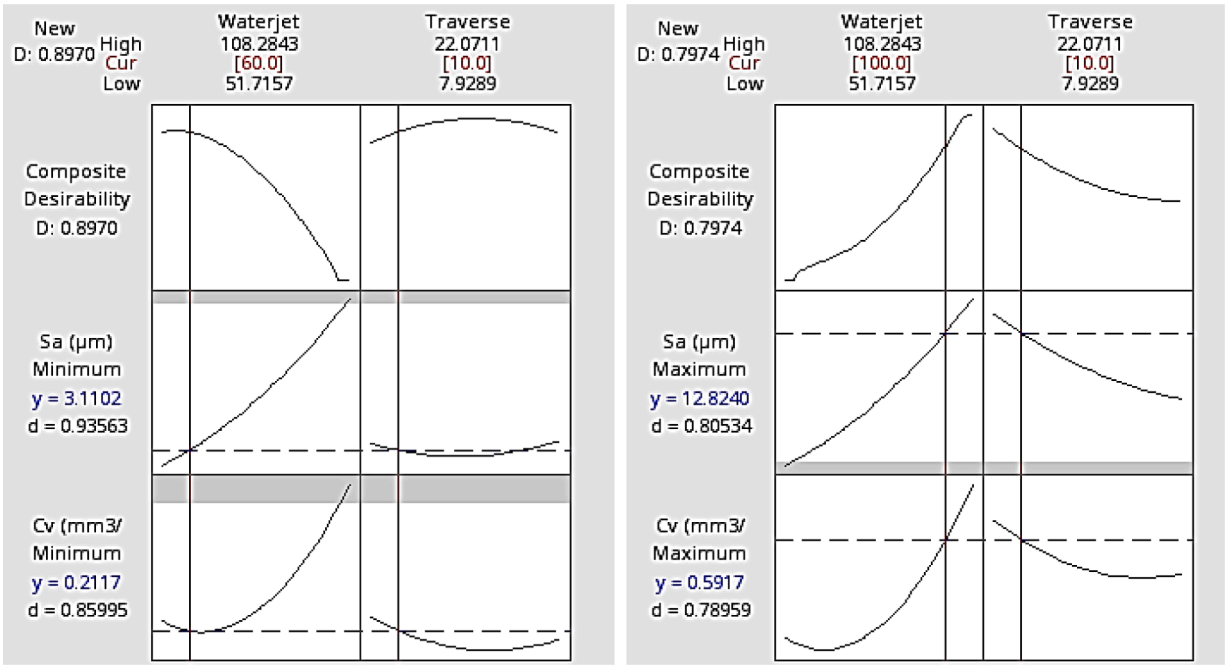

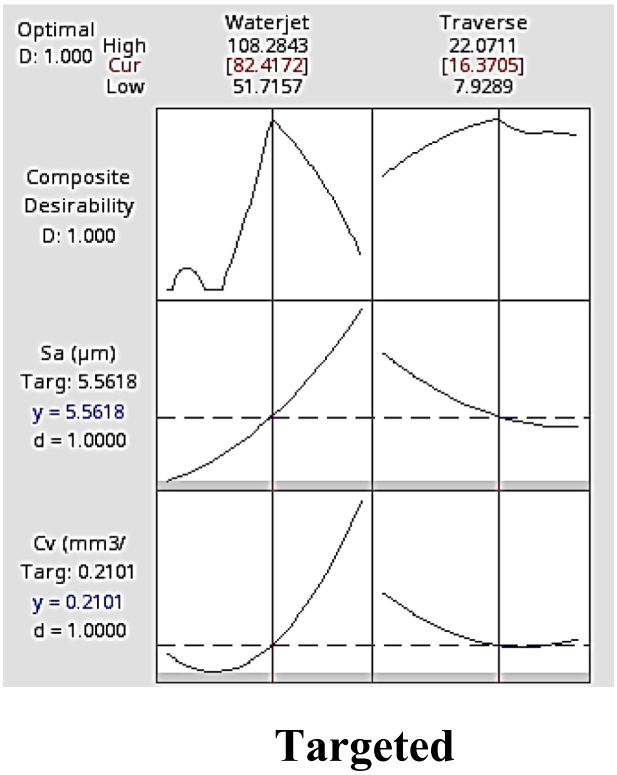

Fig. 13. Response Optimization: Sa (μm) and Cv (mm^3/cm^2) under minimum, maximum, and target conditions.

model the relationship between the factors and the responses. Subsequently, multi response optimization was performed to identify the optimal conditions for the input parameters. The response surface diagrams of the texturing outputs (Fig. 13) are predicted by the model Eqs. (1) and (2). The multi response optimization of Cv and Sa was carried out in terms of individual desirability functions that in turn are combined to obtain the composite desirability function. This composite desirability function provides the geometric mean of the individual desirability functions [42]. While this study does not explicitly constrain for specific applications, the optimized conditions imply practical use cases: high WP and low TS settings align with applications requiring higher texturing, while lower WP and higher TS are suited for cosmetic texturing.

Table 3
Predicted and experimental results under minimum, maximum and targeted conditions, along with error percentages.

Output response	Minimum condition At 60 MPa, 10 m/min		Error %	Maximum condition At 100 MPa, 10 m/min		Error %
	Predicted	Experimental		Predicted	Experimental	
Sa (μm)	3.1101	3.0531	1.86	12.8200	15.5340	17.47
Cv (mm^3/cm^2)	0.2117	0.2118	0.047	0.5917	0.6473	8.59

Targeted condition: Sa = 5.5618, Cv = 0.2101

Predicted	**Experimental**	**Error %**
82.4 MPa/16.36 m/min	80 MPa/15 m/min	3.00/9.06

$$Cv = 1.664 - 0.0354a - 0.0432b + 0.000291a^2 + 0.00158b^2 - 0.000172ab \quad (1)$$

$$Sa = -3.4 + 0.063a + 0.13b + 0.00193a^2 + 0.0222b^2 - 0.01289ab \quad (2)$$

where a represents the coded value of WP (MPa) and b represents the coded value of TS (m/min).

For the comparison between predicted and experimental data, three cases are considered: minimum, maximum, and specifically targeted conditions. These conditions are illustrated in Fig. 13 and Table 3. The Cv values for the predicted and experimental values under the minimum condition (60 MPa and 10 m/min) are 0.2117 mm^3/cm^2 and 0.2118 mm^3/cm^2, respectively. Similarly, under the maximum condition (100 MPa WP and 10 m/min TS), the Sa values are 12.8200 μm and 15.5340 μm at predicted and experimental values, respectively.

For a targeted setting with specific Sa and Cv values, a variation of only 2.4 MPa and 1.36 m/min arises between WP and TS to achieve the desired outcomes of 5.5618 μm (Sa) and 0.2101 mm^3/cm^2 (Cv). The close range of predicted values in comparison with the experimental data strengthens the significance of the developed optimization model and confirms its accuracy.

4. Conclusion

The influence of AWJ parameters, specifically waterjet pressure and traverse speed, on the surface texturing of additively manufactured continuous fiber composites was evaluated. Surface texturing parameters Cv and Sa were analyzed using 2D and 3D profiling methods. ANOVA and response surface methodology were employed for data interpretation. Scanning electron microscopy characterized surface morphology, and contamination analysis evaluated abrasive grain embedment. The key findings of this study are summarized below:

- The integration of AWJ technology with AM represents a novel attempt and innovative synergy that leverages the design freedom of AM and the versatility of AWJ, enabling precise control over texturing processes and facilitating customization with fidelity in patch fabrication for repair applications.
- WP and TS were identified as the primary influencing factors on surface texture quality, with optimal ranges of 60–100 MPa and 10–20 m/min respectively. Additionally, SS of 1 mm and SoD of 100 mm were found to ensure uniform and consistent texturing.
- The values of Cv and Sa increase with higher WP values, due to higher impact energy of the abrasive particles, while it decreases with higher TS values, because of reduced contact time at the contact surface. For a given value of TS and with increasing WP, a significant increase in Cv of 179.6 % is seen, while at a given WP and increasing TS, a decline in Cv by −8.7 % is observed.
- SEM characterization showed microcracking across the surface at lower values of WP and TS. At higher WP and TS, crater formation is also observed alongside microcracks. These findings indicate that adjusting WP and TS is crucial to balance texturing intensity with surface integrity to achieve optimum bonding surfaces.
- ANOVA analysis confirmed the influence of WP and TS on surface characteristics, with significant F-values for Cv (309.00) and Sa (2281.48) with $P < 0.05$, and low error terms (0.000410 for Cv and 0.503 for Sa), indicating robust predictive accuracy with minimal variability.
- RSM proved effective in predicting the values of Cv and Sa, with close agreement of 0.05 % and 1.86 % respectively, at lower values of WP and TS. At higher values of WP and TS, the degree of closeness was 8.59 for Cv and 17.47 % for Sa, demonstrating the accuracy of the developed RSM model.
- Contamination analysis showed that the intensity of abrasive particle deposition significantly increases at higher WP and lower TS owing to higher impact energy and prolonged interaction time. The reasons for contamination may be driven by a combination of factors, including a softer and porous matrix, non-homogeneity in specimens due to MEX process, and action of impact energy of the jet.

CRediT authorship contribution statement

Arjun Chandra Shekar: Writing – original draft, Visualization, Validation, Software, Methodology, Investigation, Formal analysis, Data curation, Conceptualization. **Atef Sawalmeh:** Software, Formal analysis. **Redouane Zitoune:** Writing – review & editing, Validation, Supervision, Resources, Project administration, Methodology, Conceptualization. **Lucas A. Hof:** Writing – review & editing, Validation, Supervision, Resources, Project administration, Methodology, Funding acquisition, Conceptualization.

Declaration of competing interest

The authors declare that they have no known competing financial interests or personal relationships that could have appeared to influence the work reported in this paper.

Acknowledgements

The authors acknowledge the financial assistance provided by Réseau de Recherche en Économie Circulaire du Québec (RRECQ), École de technogie supérieure's grant for the development of international research collaborations and Mitacs for the Globalink Research Award (IT34850). The authors also acknowledge the financial support of the Natural Sciences and Engineering Research Council of Canada (NSERC) under the Discovery Grant (RGPIN-2019-05973). Additionally, the authors thank the support received from Jean-Philippe Leclair, Thiago Lara Luiz Oliveira, and Philippe Blais during the fabrication and texturing of the samples, respectively.

Appendix A. Supplementary material

Supplementary material to this article can be found online at http

s://doi.org/10.1016/j.compositesa.2024.108698.

Data availability

Data will be made available on request.

References

[1] Rajak DK, Wagh PH, Linul E. Manufacturing technologies of carbon/glass fiber-reinforced polymer composites and their properties: a review. Polymers 2021;13:3721. https://doi.org/10.3390/polym13213721.

[2] Kalyanasundaram D, Gururaja S, Prabhune P, Singh D. Open hole fatigue testing of laser machined MD-CFRPs. Compos A Appl Sci Manuf 2018;111:33–41. https://doi.org/10.1016/j.compositesa.2018.05.005.

[3] Ivančević D, Ratković J, Giannaros E. Strain rate-dependent failure modelling of impact damage in laminated CFRP structures. Compos Struct 2024;330:117817. https://doi.org/10.1016/j.compstruct.2023.117817.

[4] Rocha H, Semprimoschnig C, Nunes JP. Sensors for process and structural health monitoring of aerospace composites: a review. Eng Struct 2021;237:112231. https://doi.org/10.1016/j.engstruct.2021.112231.

[5] Easy access rules for acceptable means of compliance for airworthiness of products, parts and appliances (AMC-20) – initial issue & amendment 1–20. EASA; 2021. https://www.easa.europa.eu/en/document-library/easy-access-rules/online-publications/easy-access-rules-acceptable-means [accessed March 2, 2024].

[6] Guidelines for the development of process specifications, instructions, and controls for the fabrication of fiber-reinforced polymer composites; n.d. https://apps.dtic.mil/sti/citations/ADA413644 [accessed July 31, 2024].

[7] Katnam KB, Da Silva LFM, Young TM. Bonded repair of composite aircraft structures: A review of scientific challenges and opportunities. Prog Aerosp Sci 2013;61:26–42. https://doi.org/10.1016/j.paerosci.2013.03.003.

[8] Delpla V, Kenné J-P, Hof LA. Circular manufacturing 4.0: towards internet of things embedded closed-loop supply chains. Int J Adv Manuf Technol 2022;118:3241–64. https://doi.org/10.1007/s00170-021-08058-3.

[9] Mejía-Moncayo C, Kenné J-P, Hof LA. On the development of a smart architecture for a sustainable manufacturing-remanufacturing system: a literature review approach. Comput Ind Eng 2023;180:109282. https://doi.org/10.1016/j.cie.2023.109282.

[10] Abbate E, Mirpourian M, Brondi C, Ballarino A, Copani G. Environmental and economic assessment of repairable carbon-fiber-reinforced polymers in circular economy perspective. Materials 2022;15:2986. https://doi.org/10.3390/ma15092986.

[11] Hall ZEC, Liu J, Brooks RA, Liu H, Crocker JWM, Joesbury AM, et al. The effectiveness of patch repairs to restore the impact properties of carbon-fibre reinforced-plastic composites. Eng Fract Mech 2022;270:108570. https://doi.org/10.1016/j.engfracmech.2022.108570.

[12] Sourd X, Zitoune R, Crouzeix L, Coulaud M, Lamouche D. Influence of the damage generated by abrasive water jet texturing on the tensile static and fatigue behaviour of 3D woven composite in the context of repair. Compos A Appl Sci Manuf 2021;149:106567. https://doi.org/10.1016/j.compositesa.2021.106567.

[13] de Freese J, Holtmannspötter J, Raschendorfer S, Hofmann T. End milling of Carbon Fiber Reinforced Plastics as surface pretreatment for adhesive bonding – effect of intralaminar damages and particle residues. J Adhes 2020.

[14] Rodrigues D, Lavorato P. Maintenance, repair and overhaul (MRO) fundamentals and strategies: an aeronautical industry overview. IJCA 2016;135:21–9. https://doi.org/10.5120/ijca2016908563.

[15] Xu J, Geier N, Shen J, Krishnaraj V, Samsudeensadham S. A review on CFRP drilling: fundamental mechanisms, damage issues, and approaches toward high-quality drilling. J Mater Res Technol 2023;24:9677–707. https://doi.org/10.1016/j.jmrt.2023.05.023.

[16] Thakur RK, Singh KK. Evaluation of advanced machining processes performance on filler-loaded polymeric composites: a state-of-the-art review. J Braz Soc Mech Sci Eng 2021;43:300. https://doi.org/10.1007/s40430-021-03027-z.

[17] Shen Z, Lu L, Sun J, Yang F, Tang Y, Xie Y. Wear patterns and wear mechanisms of cutting tools used during the manufacturing of chopped carbon fiber. Int J Mach Tool Manuf 2015;97:1–10. https://doi.org/10.1016/j.ijmachtools.2015.06.008.

[18] Shu S, He Y, Li W, He W, Zhou L, Pan X, et al. A high bonding tensile strength of CFRP ultrafast laser surface texturing method for surface damage repair. Opt Laser Technol 2025;180:111601. https://doi.org/10.1016/j.optlastec.2024.111601.

[19] Mazarbhuiya RM, Dutta H, Debnath K, Rahang M. Surface modification of CFRP composite using reverse-EDM method. Surf Interfaces 2020;18:100457. https://doi.org/10.1016/j.surfin.2020.100457.

[20] Hejjaji A, Singh D, Kubher S, Kalyanasundaram D, Gururaja S. Machining damage in FRPs: Laser versus conventional drilling. Compos A Appl Sci Manuf 2016;82:42–52. https://doi.org/10.1016/j.compositesa.2015.11.036.

[21] Dutta H, Debnath K, Sarma DK. A study of material removal and surface characteristics in micro-electrical discharge machining of carbon fiber-reinforced plastics. Polym Compos 2019;40:4033–41. https://doi.org/10.1002/pc.25264.

[22] Teicher U, Müller S, Münzner J, Nestler A. Micro-EDM of carbon fibre-reinforced plastics. Procedia CIRP 2013;6:320–5. https://doi.org/10.1016/j.procir.2013.03.092.

[23] Hejjaji A, Zitoune R, Toubal L, Crouzeix L, Collombet F. Influence of controlled depth abrasive water jet milling on the fatigue behavior of carbon/epoxy composites. Compos A Appl Sci Manuf 2019;121:397–410. https://doi.org/10.1016/j.compositesa.2019.03.045.

[24] Sourd X, Zitoune R, Crouzeix L, Coulaud M. Influence of the texturing quality consecutive to Abrasive Water Jet machining on the adhesive properties in mode I of 3D woven composite assemblies. Compos B Eng 2022;242:110091. https://doi.org/10.1016/j.compositesb.2022.110091.

[25] Sourd X, Zitoune R, Crouzeix L, Salem M, Charlas M. New model for the prediction of the machining depth during milling of 3D woven composite using abrasive waterjet process. Compos Struct 2020;234:111760. https://doi.org/10.1016/j.compstruct.2019.111760.

[26] Kumar D, Gururaja S. Abrasive waterjet machining of Ti/CFRP/Ti laminate and multi-objective optimization of the process parameters using response surface methodology. J Compos Mater 2020;54:1741–59. https://doi.org/10.1177/0021998319884611.

[27] Kashfuddoja M, Ramji M. Design of optimum patch shape and size for bonded repair on damaged Carbon fibre reinforced polymer panels. Mater Des (1980–2015) 2014;54:174–83. https://doi.org/10.1016/j.matdes.2013.08.043.

[28] Feng W, Xu F, Yuan J, Zang Y, Zhang X. Focusing on in-service repair to composite laminates of different thicknesses via scarf-repaired method. Compos Struct 2019;207:826–35. https://doi.org/10.1016/j.compstruct.2018.09.096.

[29] DA Rahito W, Azman AH. Additive manufacturing for repair and restoration in remanufacturing: an overview from object design and systems perspectives. Processes 2019;7:802. https://doi.org/10.3390/pr7110802.

[30] Rashvand K, Eder MA, Sarhadi A. In-situ and adhesive repair of continuous fiber composites using 3D printing. Addit Manuf 2024;80:103975. https://doi.org/10.1016/j.addma.2024.103975.

[31] Hou J, Lu L, Yuan S, Zhai R, Hu Y, Wang D, et al. In situ repairing of continuous fiber-reinforced thermoplastic composite via multi-axial additive manufacturing. Int J Adv Manuf Technol 2024;132:853–72. https://doi.org/10.1007/s00170-024-13381-6.

[32] Li L, Liu W, Wang Y, Zhao Z. Mechanical performance and damage monitoring of CFRP thermoplastic laminates with an open hole repaired by 3D printed patches. Compos Struct 2023;303:116308. https://doi.org/10.1016/j.compstruct.2022.116308.

[33] Ghebretinsae F, Mikkelsen O, Akessa AD. Strength analysis of 3D printed carbon fibre reinforced thermoplastic using experimental and numerical methods. IOP Conf Ser: Mater Sci Eng 2019;700:012024. https://doi.org/10.1088/1757-899X/700/1/012024.

[34] van de Werken N, Reese MS, Taha MR, Tehrani M. Investigating the effects of fiber surface treatment and alignment on mechanical properties of recycled carbon fiber composites. Compos A Appl Sci Manuf 2019;119:38–47. https://doi.org/10.1016/j.compositesa.2019.01.012.

[35] Rowe A, Pramanik A, Basak AK, Prakash C, Subramaniam S, Dixit AR, et al. Effects of abrasive waterjet machining on the quality of the surface generated on a carbon fibre reinforced polymer composite. Machines 2023;11:749. https://doi.org/10.3390/machines11070749.

[36] Vijayananth K, Pudhupalayam Muthukutti G, Keerthiveettil Ramakrishnan S, Venkatesan S, Zhou W. An integrated CRITIC-COPRAS approach for multi-response optimization on AWJM of hybrid filler–reinforced polymer composite and its surface integrity. Int J Adv Manuf Technol 2024. https://doi.org/10.1007/s00170-024-13267-7.

[37] Ganesan D, Salunkhe S, Panghal D, Murali AP, Mahalingam S, Tarigonda H, et al. Optimization of abrasive water jet machining process parameters on onyx composite followed by additive manufacturing. Processes 2023;11:2263. https://doi.org/10.3390/pr11082263.

[38] Hashish M. Optimization factors in abrasive-waterjet machining. J Eng Ind 1991;113:29–37. https://doi.org/10.1115/1.2899619.

[39] Schwartzentruber J, Papini M, Spelt JK. Characterizing and modelling delamination of carbon-fiber epoxy laminates during abrasive waterjet cutting. Compos A Appl Sci Manuf 2018;112:299–314. https://doi.org/10.1016/j.compositesa.2018.06.014.

[40] Sourd X, Zitoune R, Hejjaji A, Salem M, Crouzeix L, Lamouche D. Multi-scale analysis of the generated damage when machining pockets of 3D woven composite for repair applications using abrasive water jet process: contamination analysis. Compos A Appl Sci Manuf 2020;139:106118. https://doi.org/10.1016/j.compositesa.2020.106118.

[41] Pourrahimi S, Hof LA. On the post-processing of complex additive manufactured metallic parts: a review. Adv Eng Mater n.d.;n/a:2301511. https://doi.org/10.1002/adem.202301511.

[42] Jesthi DK, Nayak RK. Sensitivity analysis of abrasive air-jet machining parameters on machinability of carbon and glass fiber reinforced hybrid composites. Mater Today Commun 2020;25:101624. https://doi.org/10.1016/j.mtcomm.2020.101624.